ACS APPLIED MATERIALS & INTERFACES

Research Article

www.acsami.org

Manipulation of Magnetic State in Armchair Black Phosphorene Nanoribbon by Charge Doping

M. Umar Farooq, Arqum Hashmi, and Jisang Hong*

Department of Physics, Pukyong National University, Busan 608-737, Korea

Supporting Information

ABSTRACT: Using first-principles studies, we investigated the width-dependent magnetic properties of armchair black phosphorene nanoribbons (APNRs) by controlling the electron charge doping. In the unrelaxed APNRs the antiferromagnetic coupling between two phosphorus atoms in the same edge was found. However, the edge magnetic moment vanished after structure relaxation, and all of the APNRs showed a semiconducting feature. Interestingly, the charge doping substantially altered the band structures of the APNRs because the metallic states reappeared in the charge-doped APNRs. Besides this, the magnetic moment was found in the charge-doped systems. We found that the Stoner condition could nicely explain the magnetic moment at the edge atoms. Moreover, we propose that the edge-to-edge magnetic coupling can be manipulated by charge doping because the transition from the antiferromagnetic to ferromagnetic state was achieved. Our findings may bring interesting issues for spintronics applications.

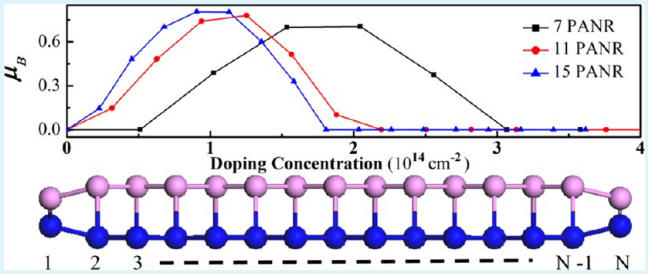

KEYWORDS: *charge doping, phosphorene, magnetism, armchair nanoribbons, doping-induced magnetism, magnetic nanoribbons*

INTRODUCTION

Material that is two-dimensional (2D) displays many intriguing physical properties and is not found in a bulk structure because its electronic structure is substantially altered from its three-dimensional characteristics. Among various types of 2D materials, graphene has attracted extensive research efforts due to its potential innovative device applications and unique physical properties. Recently, another structure of 2D material, called black phosphorus, has drawn considerable attention owing to the successful exfoliation of few-layer black phosphorus (phosphorene),[1−4] similar to graphene. Unlike the free-standing graphene, this 2D phosphorene layer has a direct band gap, and it has remarkable physical properties. For instance, few-layer black-phosphorene-based field effect transistors displayed high mobility and a high current on/off ratio. Furthermore, anisotropic electrical and optical properties have been found regarding the armchair and zigzag directions. Owing to these unusual physical properties, the phosphorene is considered a potential candidate for next-generation 2D material for electronics or optical device applications.[5−9] One can find several recent theoretical and experimental works on black phosphorus layers,[10−17] nanotubes, and nanoribbons.[18,19] These studies reveal that the band structure strongly depends on geometry and chirality.

Because the phosphorene layer is composed of nonmagnetic phosphorus atoms, no magnetic state appeared in the 2D system. The same argument can apply to the graphene because the carbon atom is also a nonmagnetic element. Nonetheless, numerous studies discussed the potential edge magnetism of zigzag graphene nanoribbons. In zigzag graphene nanoribbons, it was shown that two adjacent carbon atoms in the same edge have ferromagnetic (FM) coupling, but an antiferromagnetic (AFM) coupling prevails between two edges up to a certain edge-to-edge distance. Motivated by many studies on the edge magnetism of zigzag graphene nanoribbons, the edge magnetism was also explored in the zigzag black phosphorene nanoribbons. The zigzag phosphorene nanoribbons displayed a magnetic state at the edge atoms without the Peierls distortion. However, the edge magnetism of zigzag nanoribbons disappeared after the Peierls distortion.[20] Besides this, the edge magnetism of armchair phosphorene nanoribbons (APNRs) has also been investigated, but no report on the spin-polarized states at the edge atoms exists so far.[21] Overall, these results show that the electronic band structure and edge magnetism strongly depend on the geometry of the material. Because no published reports on the potential ferromagnetic armchair phosphorene nanoribbons are available, in this study we aim to explore the potential edge magnetism of armchair phosphorene nanoribbons. It was reported that external charge carriers can tune the magnetic interaction in dilute magnetic semiconductors.[22] The charge doping can be achieved by various ways, such as phosphorene/metal hybridization or donor impurity doping. According to a recent study of graphene nanoribbon on an Au substrate, the Au substrate caused a charge-doping effect in the graphene layer.[23] One can also find a recent theoretical study on metallic contacts with monolayer

Received: April 16, 2015
Accepted: June 16, 2015
Published: June 16, 2015

DOI: 10.1021/acsami.5b03284
ACS Appl. Mater. Interfaces 2015, 7, 14423−14430

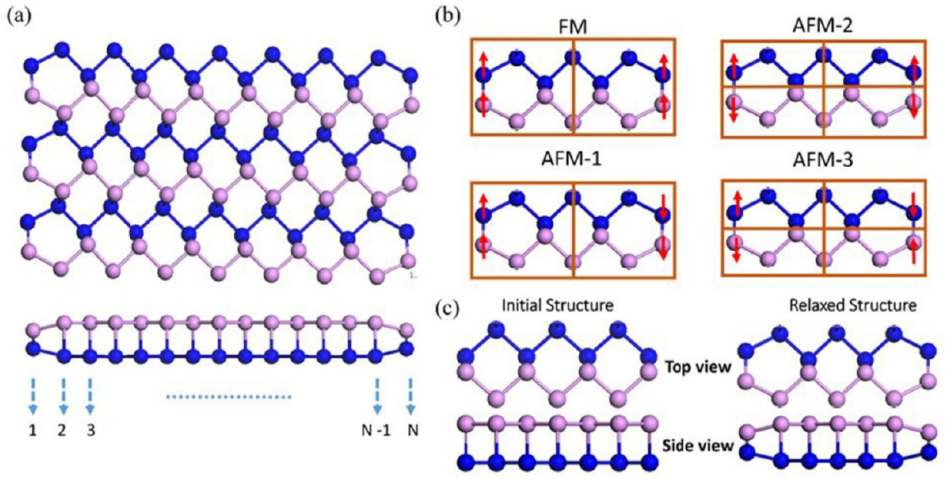

Figure 1. (a) Schematic illustration of APNR. (b) The four different magnetic configurations. (c) APNR before and after structure relaxation.

black phosphorus.[24] Of course, the substrate may affect the physical properties of the phosphorene. However, if it is a nonmagnetic substrate, its main role will be a source of hole or electron charge transfer to the layer, provided that the layer is stable on the substrate. This will result in the shift of the Fermi level and band-edge location, and so we believe that the influence of such a nonmagnetic substrate on the magnetic property enters via the Fermi level and band-edge shifting. Thus, in our work, we assumed that the charge-carrier doping was obtained by means of some suitable method. Therefore, we will explore the influence of structure relaxation on the edge magnetism, potential ferromagnetism of electron-charge-doped APNRs, and width-dependent edge-to-edge magnetic interaction.

COMPUTATIONAL DETAILS

We have performed the first-principles calculations by using the Spanish Initiative for Electronic Simulations with Thousands of Atoms (SIESTA) method.[25] Many-body effects are described within the generalized gradient approximation (GGA) by applying the Perdew–Burke–Ernzerhof (PBE) exchange-correlation functional.[26] We have used the Troullier–Martins norm-conserving pseudopotential for the treatment of core electrons. Variationally optimized double-ζ plus polarized (DZP) basis sets are used to simulate the valence electron.[27,28] Brillouin zone integration was performed with 46 k-points by using the Monkhorst–Pack k-grid scheme. A high number of k-points were used to obtain the accuracy of 0.1 meV in energy difference between the spin configurations.[29] Real-space integrations are performed on a mesh with an energy cutoff of 300 Ry. Details for the k-points and energy cutoff optimization are provided in the Supporting Information. The energy convergence criterion was kept 1×10^{-6} eV for each electronic structure calculation. The structure relaxation was performed until the force on each atom reached below the 0.01 eV/ Å. The APNRs can be obtained by cutting single-layer phosphorene along the armchair directions. The number of dimer lines can identify the width of the APNRs. Thus, we label them as *N*-APNRs, where *N* is representing a number of dimer lines. For charge-doped systems, a neutralizing jellium background of opposite charge is applied to the system to maintain the neutrality as a whole.[30,31] In our study, we have considered the 7-APNR, 11-APNR, and 15-APNR, and their corresponding widths are about 10, 17, and 24 Å, respectively.

RESULTS AND DISCUSSION

Figure 1a shows the top and side views of the nanoribbon. The blue ball represents a phosphorus atom in the lower layer, and the pink ball represents the upper layer. Because the main purpose of this report is to explore the magnetic properties of APNRs, we have considered four different spin configurations as displayed in Figure 1b. As remarked above, the Peierls distortion drastically modified the edge magnetic property of the zigzag phosphorene nanoribbon.[20] This shows that the magnetic property is subject to the edge geometry, and the same argument can apply to the armchair nanoribbons. Therefore, we have studied the geometry's effect on the edge magnetism. Figure 1c shows the geometry of the nanoribbon before and after relaxation. Except for the edge atoms, no significant change in the interatomic distance was found after structure relaxation, and the calculated bond length between two edge atoms was about 2.1 Å. For the charge-doped systems, we performed structure optimization once again after charge doping. The charge doping did not strongly disturb the interatomic distance of the edge atoms because the calculated interatomic distance at the edge was in the range of 2.14–2.16 Å depending on the charge-doping concentration. In many cases, the noncollinear spin canting appears in the hexagonal system due to triangular spin configuration. However, in our study, the structure-optimized APNRs showed a dimerized edge structure. Therefore, we only considered the collinear spin configuration. To reveal the role of structure relaxation on the edge magnetism, we first explored the total energies of unrelaxed APNRs in each spin configuration, and Table 1 presents the calculated total energy differences. We can find that two adjacent phosphorus atoms in the same edge have an antiparallel spin interaction. The major contribution to the magnetic moment originated from the edge atoms. However, the edge-to-edge magnetic interaction is negligible because the energy difference between AFM2 and AFM3 was extremely weak. Despite the antiparallel spin interaction at the edge in the unrelaxed APNRs, the relaxed structures were much more stable than the unrelaxed structures, as shown in Table 1. Furthermore, the spin-polarized state at the edge phosphorus

Table 1. Total Energy Differences (in meV/cell) for Different Magnetic Configurations

ribbon	E_{NM-FM}	$E_{FM-AFM1}$	$E_{FM-AFM2}$	$E_{AFM2-AFM3}$	$E_{unrelaxed-relaxed}$
7-APNR	118.597	−8.581	129.021	0.595	1518.685
11-APNR	138.930	−1.582	163.506	−0.781	1577.038
15-APNR	143.493	0.284	162.392	−0.005	1617.982

DOI: 10.1021/acsami.5b03284
ACS Appl. Mater. Interfaces 2015, 7, 14423–14430

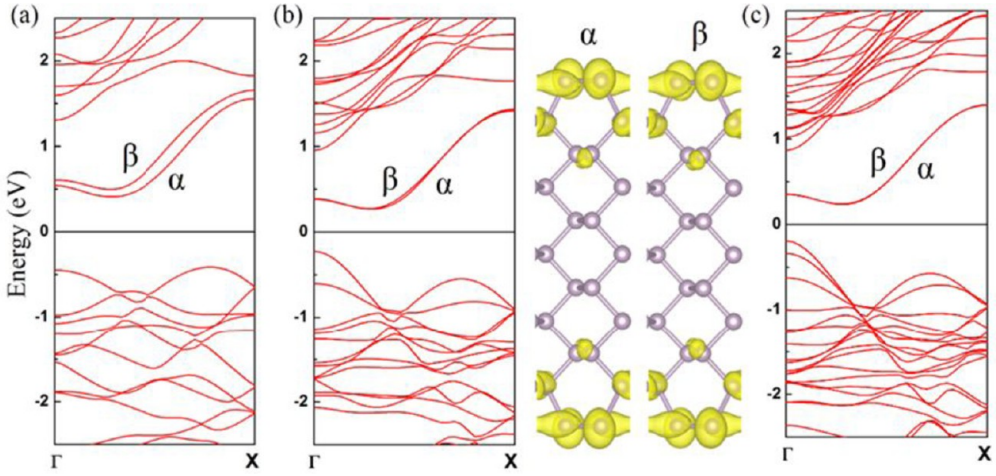

Figure 2. Calculated band structures after structure relaxation. The α and β labels are indicating the edge states (a) 7-APNR, (b) 11-APNR with isosurface plots of the wave function square modulus at the Γ-point, and (c) 15-APNR.

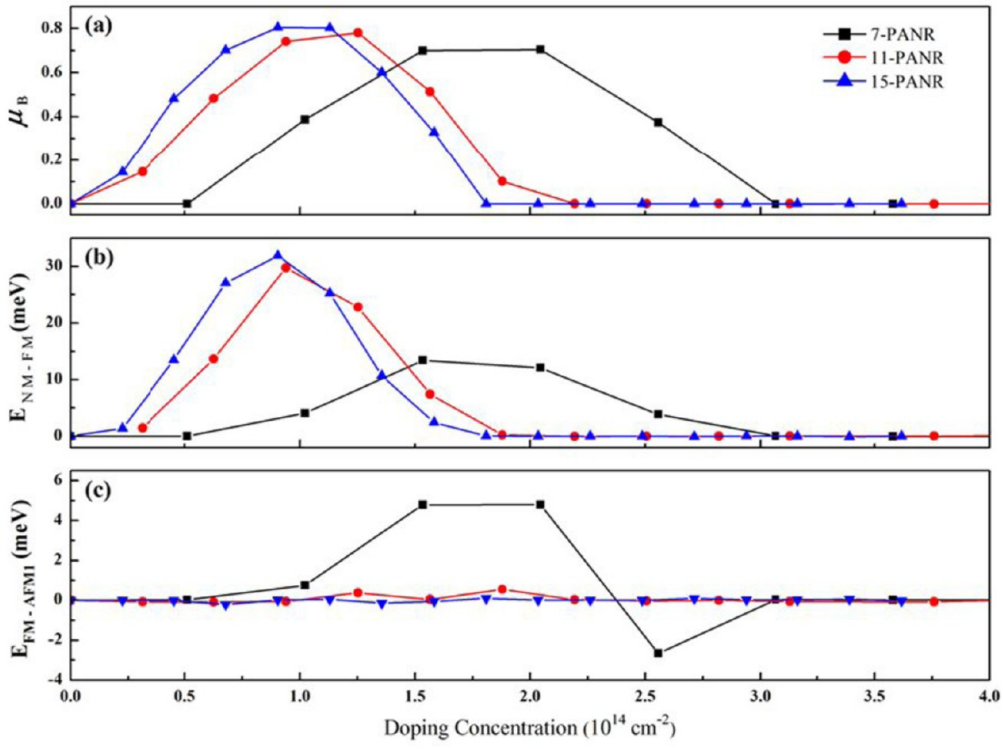

Figure 3. (a) Magnetic moment per unit cell in the FM configuration. (b) The total energy difference between the NM and FM states. (c) The total energy difference between the FM and AFM1 states. Here, the unit of the charge doping concentration is 10^{14} cm^{-2}.

atom disappeared. These results imply that the magnetic state is sensitive to the geometry optimization.

Figure 2a–c presents the band structures of relaxed systems where we found a semiconducting feature. There are two band dispersions in the conduction band, named as α and β, arising from the edge states. The isosurface plots of the wave function square modulus belonging to α and β for 11-APNR are shown in Figure 2b. One can clearly see that these states are identical, localized at the edge, and delocalized along the periodic direction. The energy gap shows a decreasing tendency as the width of the ribbon increases. This is a typical quantum confinement effect because the energy level spacing is inversely proportional to the width of nanoribbon. Moreover, the relaxed nanoribbons show no spin-polarized state, and this feature was independent of the width of the nanoribbons. In the unrelaxed nanoribbons, we found dangling bonds at the edges, and this resulted in a spin-polarized state. However, the dangling bond disappeared after structure relaxation, and this resulted in a nonmagnetic state. Overall, our finding implies that the magnetic property of armchair nanoribbons vanishes due to the completion of the dangling bond after structure relaxation.

Because the structure-optimized systems do not show a spin-polarized state, the potential magnetism induced by an external charge doping was explored. We found that the initial AFM2 and AFM3 spin configurations converged to a nonmagnetic (NM) state after fully-self-consistent calculations. Thus, we focused on the NM, FM, and AFM1 spin configurations and calculated the magnetic moment at the edge atoms. For AFM1

DOI: 10.1021/acsami.5b03284
ACS Appl. Mater. Interfaces 2015, 7, 14423–14430

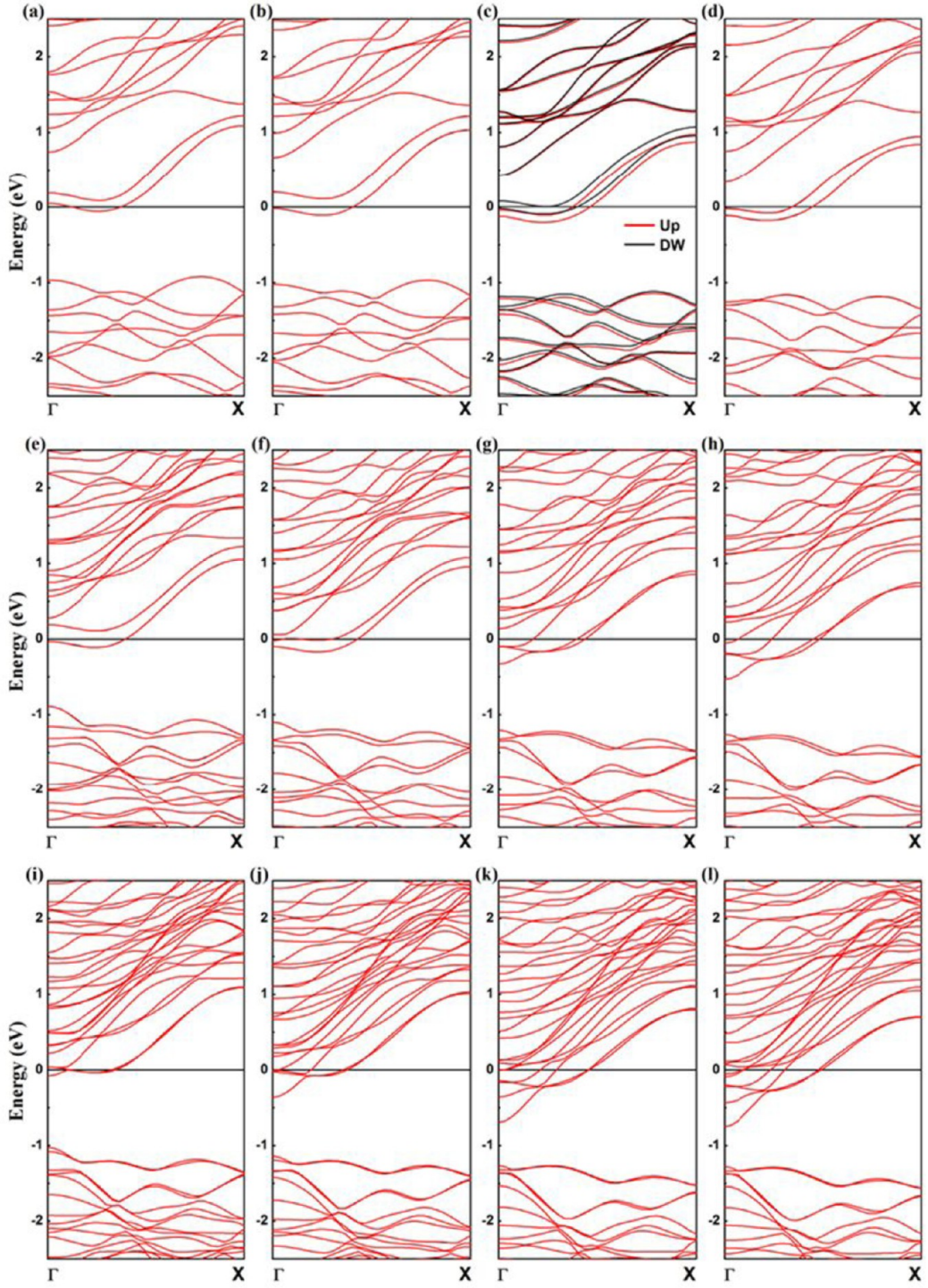

Figure 4. Calculated band structures of the most stable magnetic state. Panels a–d are for 7-APNR at 1.0×10^{14}, 1.5×10^{14}, 2.5×10^{14}, and 3.1×10^{14} cm^{-1} doping concentrations, respectively. Panels e–h are for 11-APNR at 9.4×10^{14}, 1.6×10^{14}, 2.5×10^{14}, and 3.1×10^{14} cm^{-1} doping concentrations, respectively. Panels i–l are for 15-APNR at 9.0×10^{14}, 1.6×10^{14}, 2.5×10^{14}, and 3.2×10^{14} cm^{-1} doping concentrations, respectively. The red and black lines are for the up and down spins, respectively.

configurations, the net magnetic moment will vanish because the magnetic moment of one half of the unit cell is opposite to that of the other half of the unit cell. We found that the magnetic moment of the half of the unit cell in the AFM1 configuration was almost identical to that in the FM configuration. Thus, we present the results of FM spin configurations, and Figure 3a shows the calculated magnetic moment per unit cell. Very interestingly, we found a magnetic moment, although it depends on the width of the ribbons and charge-doping concentration. The major contribution to the magnetic moment originated from the edge atoms. Note that the inner layer atoms next to the edge atoms also have an induced spin-polarized state, but the magnitude was relatively weak compared to the magnetic moment of the edge atom. Although we found that the edge atoms could have a magnetic moment, it is necessary to compare the total energies in each

DOI: 10.1021/acsami.5b03284
ACS Appl. Mater. Interfaces 2015, 7, 14423–14430

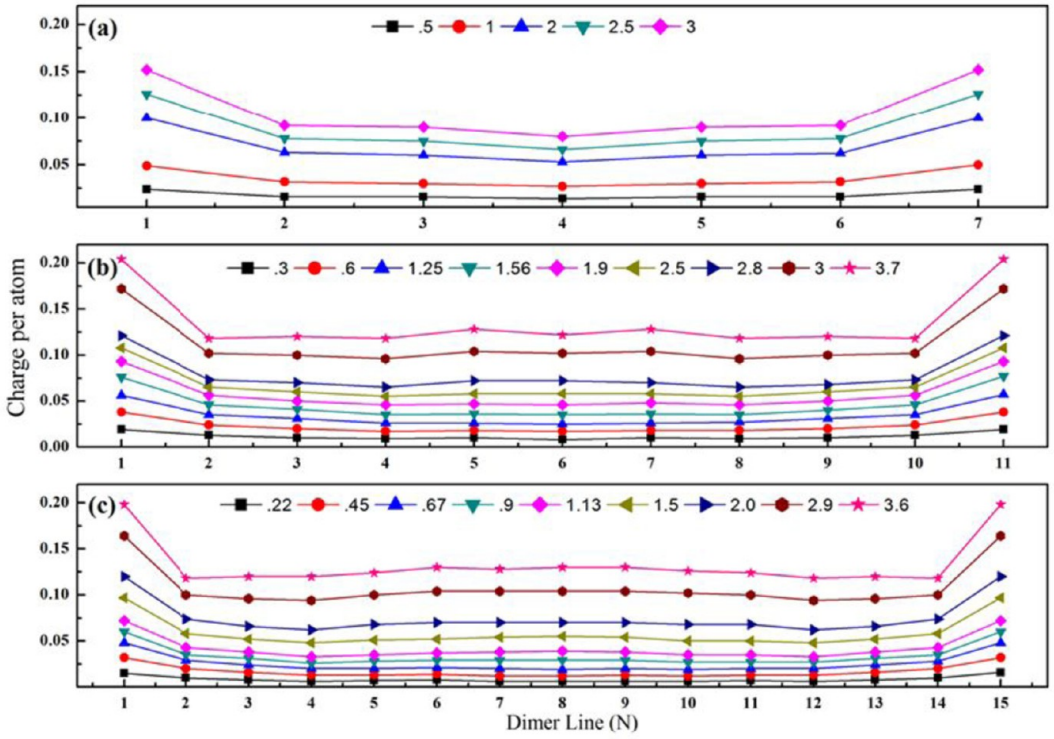

Figure 5. Doped charge accumulation in different dimer lines: (a) 7-APNR, (b) 11-APNR, and (c) 15-APNR. Each line shows the different doping ratios in units of 10^{14} cm^{-2}.

magnetic configuration for obtaining a true ground state. Figure 3b shows the total energy difference between the NM and FM spin configurations. It is clearly shown that the spin-polarized state is more stable than the nonmagnetic state as long as the magnetic moment exists, although the energy difference depends on the charge-doping concentration. As described in Figure 3b, the FM state was more stable than the NM state. Thus, we now investigate the magnetic stability between the FM and AFM1 states. Figure 3c presents the total energy difference of the FM and AFM1 configurations. In 11-APNR and 15-APNR, the energy difference almost vanishes. This shows that the edge-to-edge magnetic interaction in 11-APNR and 15-APNR is negligible. The unrelaxed zigzag phosphorene nanoribbons maintained the edge-to-edge magnetic interaction up to a width of 5 nm. However, as displayed in Table 1, the edge-to-edge magnetic interaction vanished in a much shorter width. Indeed, the edge-to-edge direction in APNR corresponds to the zigzag direction in the 2D layer, while the edge-to-edge direction in zigzag nanoribbon is the same as the armchair direction in the 2D layer. It has been shown that the valence bandwidth of the 2D layer along the armchair direction is much broader than the zigzag direction.[2] This implies that the states in the zigzag direction are more localized than the armchair direction. Therefore, the effective spin interaction between two edges (along the zigzag direction) in APNRs diminished faster than that in zigzag nanoribbons. However, we found an interesting feature in 7-APNR. In this 7-APNR nanoribbon, the edge-to-edge magnetic interaction survived, and more surprisingly, an FM ground state was achieved at some charge-doping concentrations. Indeed, numerous studies investigated the edge-to-edge magnetic interaction in zigzag graphene nanoribbons. In general, the edge-to-edge coupling had an antiferromagnetic state, although the energy difference between FM and AFM was dependent on the width of the graphene nanoribbon. In addition, it was shown that the energy difference between the FM and AFM states became almost 0 when the width of the graphene nanoribbon was 6 nm.[32] In the graphene nanoribbons, the antiferromagnetic interaction was ascribed to the effect of the magnetic tails of the localized state, as discussed in relation to the graphene nanoribbons. Thus, the edge-to-edge magnetic interaction in 7-APNR may be explained in the same manner. However, in our armchair phosphorene nanoribbons, it seems that the charge doping modulates the details of subtle edge-to-edge coupling because the charge doping can alter the ground-state magnetic phase. We now show the band structure of ground state APNRs. Figure 4 displays the calculated band structures with different charge-doping ratios. As displayed in Figure 2, at zero-charge doping, the relaxed nanoribbons showed a semiconducting feature, and this agrees with previous results.[21] However, external charge doping drastically altered the electronic band structure. We found metallic states in the APNRs, and this was independent of the spin configuration at the edges. In addition, the general band shapes are not affected by the charge doping, but the external charge doping simply induced a shift of the Fermi level, although the low-lying bands display minor changes with the variation in the charge-doping concentration. Overall, we determined that the metallic band shapes seem very rigid.

It will be interesting to know the external charge distribution. Thus, we calculated the charge population at every atomic position for different charge doping concentrations. Figure 5 shows the calculated results. At zero-charge doping, a uniform charge distribution took place because no meaningful charge accumulation in any atom was observed, and this feature was independent of the width of the nanoribbon. However, with external charge doping in each nanoribbon, a common feature was extracted. We found a noticeable charge accumulation near the edge atoms, but the external charge was almost uniformly

DOI: 10.1021/acsami.5b03284
ACS Appl. Mater. Interfaces 2015, 7, 14423−14430

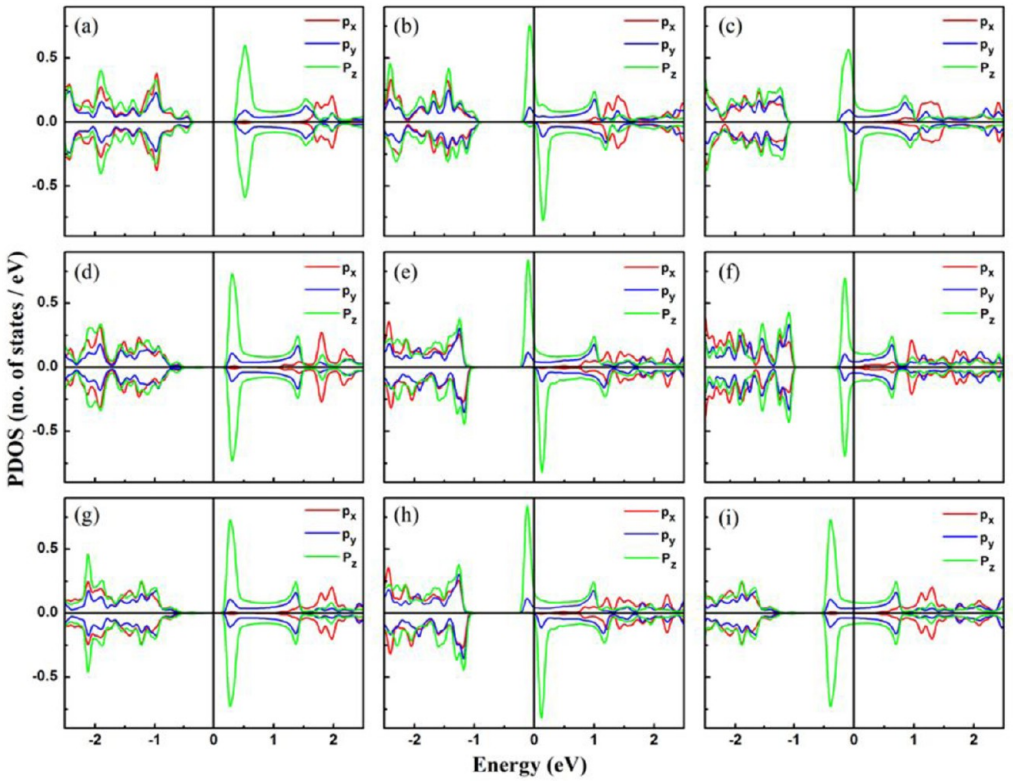

Figure 6. Calculated DOS of edge atoms of (a) 7-APNR at zero doping, (b) 7-APNR at 1.5×10^{14} cm^{-2}, (c) 7-APNR at 2.56×10^{14} cm^{-2}, (d) 11-APNR at zero doping, (e) 11-APNR at 1.25×10^{14} cm^{-2}, (f) 11-APNR at 2.80×10^{14} cm^{-2}, (g) 15-APNR at zero doping, (h) 15-APNR at 1.25×10^{14} cm^{-2}, and (i) 15-APNR at 3×10^{14} cm^{-2}.

distributed in the inner layers. To understand the origin of a magnetic state due to this charge accumulation at the edge atoms, we now show the calculated density of states (DOS) of the edge atoms in Figure 6 at various charge doping concentrations. Figure 6a,d,g shows the DOS without any charge doping for the 7-APNR, 11-APNR, and 15-APNR. From the calculated band structures, it is clear that the first peak in the DOS originates from the edge states called α and β, shown in Figure 2. Due to the chiral symmetry, we only presented the DOS of one edge atom because the other edge atom has the same features in the FM spin configuration. In the AFM1 configuration, two opposite edges show the reversed DOS characteristic. The DOS reveals that a major contribution to the magnetic moment of the edge atom originates from the p_z orbital, and minor contributions to the magnetic moment from other orbitals are observed. By further increasing the charge-doping concentration in 11-APNR and 15-APNR, the spin-asymmetric DOS has disappeared. This means that the edge atom does not have any magnetic moment. However, in 7-APNR, we still observe a spin-polarized state in a more enhanced range of doping concentration. Even in this case, we find that the major contribution to the magnetic moment originates from the p_z orbital. As described in the band structures, the low-lying bands crossed the Fermi level, and this resulted in a metallic state. We found that this metallic feature originated from the edge atom because the DOS of inner layers near the Fermi level was quite weak. Furthermore, the calculated DOS spectral shape may reveal the origin of the edge magnetism. According to the Stoner criterion, the magnetic state becomes more stable than nonmagnetic state when the Fermi level is positioned at a high peak of DOS. As displayed in the DOS and band structures, the general shapes of the band structure and DOS are unchanged, but the Fermi level is shifted as the charge-doping concentration varied. Thus, the introducing of external charge mainly contributes to the shift of the Fermi level. It is clearly displayed that the magnetic state appears at the edge atom when this Fermi level is positioned at the peak of the DOS. Beyond this high peak of DOS in 11-APNR and 15 APNR, the Fermi level is placed at a low DOS. Thus, the edge magnetism vanished. Consequently, the Stoner condition can nicely account for the existence of a magnetic moment in armchair nanoribbons.

CONCLUSIONS

In conclusion, we have investigated the magnetic properties of APNRs. The influence of structural relaxation and external charge doping on the edge magnetism were explored by changing the width of the nanoribbons. The edge magnetic state appeared in the unrelaxed APNRs, and the phosphorus atoms located along an edge line had an antiparallel spin coupling. Nonetheless, we found no meaningful edge-to-edge magnetic interaction. We found semiconducting band gaps in the APNRs, and the edge magnetism disappeared after structural relaxation. Indeed, we observed a dangling bond in unrelaxed nanoribbons, but this dangling bond vanished due to the effect of structure optimization. Surprisingly, we found that the external charge doping significantly altered the electronic band structure and magnetic properties. The energy gap observed in undoped APNRs vanished, and the metallic band structure appeared after charge doping. Furthermore, the edge magnetic state was also obtained after charge doping, although the size of the magnetic moment was dependent on the width

DOI: 10.1021/acsami.5b03284
ACS Appl. Mater. Interfaces 2015, 7, 14423−14430

and charge doping concentration, and the magnetic state was more stable than the nonmagnetic state. The major contribution to the magnetic moment originated from the edge atoms, and mostly the p_z orbital played an essential role in the edge magnetism. The edge-to-edge magnetic interaction was very weak, and we found no meaningful energy difference between the FM and AFM1 states in 11 and 15 APNRs. However, the edge-to-edge magnetic interaction survived in 7-APNR. More surprisingly, the possibility of FM armchair nanoribbon was addressed because we found an FM ground state at some charge-doping concentrations in the 7-APNR. The magnetic interaction may be ascribed to the effect of magnetic tails of the localized state, as explained for graphene nanoribbons, and it seems that the charge doping can manipulate the details of the magnetic interaction. We also found that the Stoner condition could nicely account for the origin of the magnetic state at the edge atoms. Overall, we predict the potential for ferromagnetic armchair nanoribbon, and this finding may bring up an intriguing issue regarding the spintronics applications.

■ ASSOCIATED CONTENT

Supporting Information

Plots of the number of k-points and the optimized energy cutoff values. The Supporting Information is available free of charge on the ACS Publications website at DOI: 10.1021/acsami.5b03284.

■ AUTHOR INFORMATION

Corresponding Author

*E-mail: hongj@pknu.ac.kr.

Notes

The authors declare no competing financial interests.

■ ACKNOWLEDGMENTS

This research was supported by the Basic Science Research Program through the National Research Foundation of Korea (NRF), funded by the Ministry of Education, Science, and Technology (no. 2013R1A1A2006071), and by the Supercomputing Center/Korea Institute of Science and Technology Information with supercomputing resources including technical support (KSC-2014-C3-071).

■ REFERENCES

(1) Li, L.; Yu, Y.; Ye, G. J.; Ge, Q.; Ou, X.; Wu, H.; Feng, D.; Chen, X. H.; Zhang, Y. Black Phosphorus Field-Effect Transistors. *Nat. Nanotechnol.* **2014**, *9*, 372−377.

(2) Liu, H.; Neal, A. T.; Zhu, Z.; Luo, Z.; Xu, X.; Tománek, D.; Ye, P. D. Phosphorene: An Unexplored 2D Semiconductor with a High Hole Mobility. *ACS Nano* **2014**, *8*, 4033−4041.

(3) Lu, W.; Nan, H.; Hong, J.; Chen, Y.; Zhu, C.; Liang, Z.; Ma, X.; Ni, Z.; Jin, C.; Zhang, Z. Plasma-Assisted Fabrication of Monolayer Phosphorene and Its Raman Characterization. *Nano Res.* **2014**, *7*, 853−859.

(4) Castellanos-Gomez, A.; Vicarelli, L.; Prada, E.; Island, J. O.; Narasimha-Acharya, K. L.; Blanter, S. I.; Groenendijk, D. J.; Buscema, M.; Steele, G. A.; Alvarez, J. V.; Zandbergen, H. W.; Palacios, J. J.; van der Zant, H. S. J. Isolation and Characterization of Few-Layer Black Phosphorus. *2D Mater.* **2014**, *1*, 025001.

(5) Liu, H.; Neal, A. T.; Zhu, Z.; Luo, Z.; Xu, X.; Tománek, D.; Ye, P. D. Phosphorene: An Unexplored 2D Semiconductor with a High Hole Mobility. *ACS Nano* **2014**, *8*, 4033−4041.

(6) Zhang, S.; Yang, J.; Xu, R.; Wang, F.; Li, W.; Ghufran, M.; Zhang, Y.-W.; Yu, Z.; Zhang, G.; Qin, Q.; Lu, Y. Extraordinary Photoluminescence and Strong Temperature/Angle-Dependent Raman Responses in Few-Layer Phosphorene. *ACS Nano* **2014**, *8*, 9590−9596.

(7) Xia, F.; Wang, H.; Jia, Y. Rediscovering Black Phosphorus as an Anisotropic Layered Material for Optoelectronics and Electronics. *Nat. Commun.* **2014**, *5*, 4458.

(8) Das, S.; Demarteau, M.; Roelofs, A. Ambipolar Phosphorene Field Effect Transistor. *ACS Nano* **2014**, *8* (11), 11730−11738.

(9) Qiao, J.; Kong, X.; Hu, Z.-X.; Yang, F.; Ji, W. High-Mobility Transport Anisotropy and Linear Dichroism in Few-Layer Black Phosphorus. *Nat. Commun.* **2014**, *5*, 4475.

(10) Khan, I.; Hong, J. Manipulation of Magnetic State in Phosphorene Layer by Non-Magnetic Impurity Doping. *New J. Phys.* **2015**, *17*, 023056.

(11) Dai, J.; Zeng, X. C. Bilayer Phosphorene: Effect of Stacking Order on Bandgap and Its Potential Applications in Thin-Film Solar Cells. *J. Phys. Chem. Lett.* **2014**, *5*, 1289−1293.

(12) Buscema, M.; Groenendijk, D. J.; Blanter, S. I.; Steele, G. A.; van der Zant, H. S. J.; Castellanos-Gomez, A. Fast and Broadband Photoresponse of Few-Layer Black Phosphorus Field-Effect Transistors. *Nano Lett.* **2014**, *14*, 3347−3352.

(13) Rudenko, A. N.; Katsnelson, M. I. Quasiparticle Band Structure and Tight-Binding Model for Single- and Bilayer Black Phosphorus. *Phys. Rev. B: Condens. Matter Mater. Phys.* **2014**, *89*, 201408.

(14) Tran, V.; Soklaski, R.; Liang, Y.; Yang, L. Layer-Controlled Band Gap and Anisotropic Excitons in Few-Layer Black Phosphorus. *Phys. Rev. B: Condens. Matter Mater. Phys.* **2014**, *89*, 235319.

(15) Fei, R.; Yang, L. Strain-Engineering the Anisotropic Electrical Conductance of Few-Layer Black Phosphorus. *Nano Lett.* **2014**, *14*, 2884−2889.

(16) Koenig, S. P.; Doganov, R. A.; Schmidt, H.; Neto, A. H. C.; Özyilmaz, B. Electric Field Effect in Ultrathin Black Phosphorus. *Appl. Phys. Lett.* **2014**, *104*, 103106.

(17) Rodin, A. S.; Carvalho, A.; Castro Neto, A. H. Strain-Induced Gap Modification in Black Phosphorus. *Phys. Rev. Lett.* **2014**, *112*, 176801.

(18) Tran, V.; Yang, L. Scaling Laws for the Band Gap and Optical Response of Phosphorene Nanoribbons. *Phys. Rev. B: Condens. Matter Mater. Phys.* **2014**, *89*, 245407.

(19) Guo, H.; Lu, N.; Dai, J.; Wu, X.; Zeng, X. C. Phosphorene Nanoribbons, Phosphorus Nanotubes, and van Der Waals Multilayers. *J. Phys. Chem. C* **2014**, *118*, 14051−14059.

(20) Zhu, Z.; Li, C.; Yu, W.; Chang, D.; Sun, Q.; Jia, Y. Magnetism of Zigzag Edge Phosphorene Nanoribbons. *Appl. Phys. Lett.* **2014**, *105*, 113105.

(21) Guo, H.; Lu, N.; Dai, J.; Wu, X.; Zeng, X. C. Phosphorene Nanoribbons, Phosphorus Nanotubes, and van Der Waals Multilayers. *J. Phys. Chem. C* **2014**, *118*, 14051−14059.

(22) Chiba, D.; Yamanouchi, M.; Matsukura, F.; Ohno, H. Electrical Manipulation of Magnetization Reversal in a Ferromagnetic Semiconductor. *Science* **2003**, *301*, 943−945.

(23) Magda, G. Z.; Jin, X.; Hagymási, I.; Vancsó, P.; Osváth, Z.; Nemes-Incze, P.; Hwang, C.; Biró, L. P.; Tapasztó, L. Room-Temperature Magnetic Order on Zigzag Edges of Narrow Graphene Nanoribbons. *Nature* **2014**, *514*, 608−611.

(24) Gong, K.; Zhang, L.; Ji, W.; Guo, H. Electrical Contacts to Monolayer Black Phosphorus: A First-Principles Investigation. *Phys. Rev. B: Condens. Matter Mater. Phys.* **2014**, *90*, 125441.

(25) Soler, J. M.; Artacho, E.; Gale, J. D.; García, A.; Junquera, J.; Ordejón, P.; Sánchez-Portal, D. The SIESTA Method for Ab Initio Order-N Materials Simulation. *J. Phys.: Condens. Matter* **2002**, *14*, 2745−2779.

(26) Perdew, J. P.; Burke, K.; Ernzerhof, M. Generalized Gradient Approximation Made Simple. *Phys. Rev. Lett.* **1996**, *77*, 3865−3868.

(27) Anglada, E.; M. Soler, J.; Junquera, J.; Artacho, E. Systematic Generation of Finite-Range Atomic Basis Sets for Linear-Scaling Calculations. *Phys. Rev. B: Condens. Matter Mater. Phys.* **2002**, *66*, 205101.

DOI: 10.1021/acsami.5b03284
ACS Appl. Mater. Interfaces 2015, 7, 14423−14430

(28) Junquera, J.; Paz, Ó.; Sánchez-Portal, D.; Artacho, E. Numerical Atomic Orbitals for Linear-Scaling Calculations. *Phys. Rev. B: Condens. Matter Mater. Phys.* **2001**, *64*, 235111.
(29) Monkhorst, H. J.; Pack, J. D. Special Points for Brillouin-Zone Integrations. *Phys. Rev. B: Condens. Matter Mater. Phys.* **1976**, *13*, 5188−5192.
(30) De Vita, A.; Gillan, M. J.; Lin, J. S.; Payne, M. C.; Štich, I.; Clarke, L. J. Defect Energetics in MgO Treated by First-Principles Methods. *Phys. Rev. B: Condens. Matter Mater. Phys.* **1992**, *46*, 12964−12973.
(31) Leslie, M.; Gillan, N. J. The Energy and Elastic Dipole Tensor of Defects in Ionic Crystals Calculated by the Supercell Method. *J. Phys. C: Solid State Phys.* **1985**, *18*, 973.
(32) Son, Y.-W.; Cohen, M. L.; Louie, S. G. Energy Gaps in Graphene Nanoribbons. *Phys. Rev. Lett.* **2006**, *97*, 216803.

DOI: 10.1021/acsami.5b03284
ACS Appl. Mater. Interfaces 2015, 7, 14423−14430